Systematics of the α-decay to rotational states

D. S. Delion,[1] S. Peltonen,[2] and J. Suhonen[2]
[1]*National Institute of Physics and Nuclear Engineering, Bucharest-Măgurele, POB MG-6, Romania*
[2]*Department of Physics, University of Jyväskylä, POB 35, FIN-40351, Jyväskylä, Finland*
(Received 28 November 2005; published 27 January 2006)

We analyze α decays to rotational states in even-even nuclei by using the stationary coupled channels approach. Collective excitations are described by the rigid rotator model. The α-nucleus interaction is given by a double folding procedure using M3Y plus Coulomb nucleon-nucleon forces. We use a harmonic oscillator repulsive potential with one independent parameter, to simulate the Pauli principle. The decaying state is identified with the first resonance inside the resulting pocketlike potential. The energy of the resonant state is adjusted to the experimental Q value by using the depth of the repulsion. We obtained a good agreement with existing experimental data concerning total half-lives and decay widths to $J = 2^+$ states by changing the factor multiplying the nucleon-nucleon interaction according to the rule $v_a = 0.668 - 0.004\,(A - 208)$. Concerning the decay widths to $J = 4^+$ states we obtained a good agreement for $Z = 90$ neutron chain and a satisfactory description for $Z = 92, 96$, and 98, chains. It is possible to improve the agreement concerning transitions to $J = 4^+$ states by considering a constant quenching strength $v_a = 0.6$ and by changing the width of the Gaussian describing the α-cluster density according to the rule $b = 1.744 - 0.032\,(A - 208)$. We found out that the computed widths to excited states are correlated with the corresponding deformation parameters. We conclude that the α-decay fine structure is a sensitive tool to probe fundamental aspects of the effective nuclear interaction and its dependence on the α clustering.

DOI: 10.1103/PhysRevC.73.014315 PACS number(s): 21.10.Tg, 23.60.+e, 24.10.Eq

I. INTRODUCTION

The importance of the Coulomb interaction for the α-decay width is well known [1]. It defines the probability for a preformed α particle to penetrate quantum-mechanically the electrostatic barrier. The relative values of half-lives can be satisfactorily described within this simple picture. To describe absolute half-lives it is also necessary to consider the α-particle spectroscopic factor, or preformation probability, multiplying the barrier penetrability. This factor was introduced within the R-matrix theory in Refs. [2–4]. It is defined by the square of the overlap between the internal wave function and the product of the daughter and α-particle wave functions.

The first systematic analysis of α-decay widths in even and odd-mass actinide nuclei was performed in Ref. [5], by using the pairing approach for the preformation probability and spherical penetration factors. Very recently we performed a systematic analysis of all measured decays between ground states by using a similar paring interaction but including single particle configurations in continuum and a deformed penetration factor. We evidenced the important role played by the preexisting α clustering [6] in addition to the shell-model preformation.

For transitions between ground states the preformation factor is a coherent superposition of many single-particle configurations, including states in continuum and therefore the decay width is not very sensitive to the nuclear structure details. The situation becomes quite different for transitions to excited states, because only those single-particle states that are around the Fermi surfaces are involved. Therefore decay widths to excited states are very sensitive to the structure of the wave function in the daughter nucleus. To separate the exponential dependence between the decay width and Q value one extracts the barrier penetration by introducing the so-called hindrance factors (HF) [7]. They define the ratio between preformation probabilities of two nuclear states.

The first attempts to compute HFs in vibrational nuclei within the quasiparticle random-phase approximation (QRPA) were performed in Refs. [8–10]. Later on, in Ref. [11] an explanation was given for the connection between the HF of the first excited 0^+ state and the neutron number for Pb isotopes. In the last decade the α-decay spectroscopy was used to investigate the 0^+ and 2^+ excited states in the Pb [12–19] and U region [20]. We analyzed some of the experimental results concerning the fine structure of 2^+ states by using the QRPA formalism in Refs. [21–23].

The first computations of the α-decay widths in rotational nuclei by using the coupled channels method were performed in Ref. [24]. In Ref. [25] HFs were estimated in rotational nuclei by using the Fröman approach [26] for the barrier penetration and a simple phenomenological ansatz for the preformation factor. The α-core potential was estimated by using the double folding procedure in Refs. [27,28] and more recently in Ref. [29]. In all these works it was concluded that the strength of the nucleon-nucleon force should be quenched (i.e., the Coulomb barrier should increase) to describe the right relation between the half-life and Q value. This kind of potential was used to estimate ground-state-to-ground-state half-lives within the spherical approach in Ref. [30]. In Ref. [31] the densities in the double-folded α-core potential were computed within the relativistic mean-field theory.

In several recent articles [32–34] we analyzed the double fine structure of emitted fragments in the cold fission of ^{252}Cf within the coupled channels formalism. The fissioning state was identified with a resonance in the interfragment potential, computed using the already-mentioned double

folding procedure. For the external part of the potential we used the two-body M3Y plus Coulomb interaction. The energy was adjusted to reproduce the experimental Q value by using an internal repulsive core. We found out that the yields to excited states in both fragments are very sensitive to nuclear structure details such as the mean-field deformation and density diffusivity. Unfortunately there are only few available experimental data to be analyzed in this field [35].

However, there are a lot of high-precision data on α-decay fine structure to rotational levels, see, e.g., Ref. [36]. The aim of this article is to apply the coupled channels technique, used to describe double fine structure in cold fission, in the simpler case of α decay. In this way we can test to what extent the microscopically computed interfragment potential is able to describe not only the total decay width but also the very complex picture of decay widths to rotational levels.

The article is organized according to the following plan: In Sec. II we shortly remind the main ingredients of the stationary coupled channels formalism describing α-decay fine structure to rotational states. In Sec. III we analyze the influence of the attractive and repulsive parts of the potential on the decay widths. In Sec. IV we give a systematics on measured α-decay widths. In the last section we draw conclusions.

II. THEORETICAL BACKGROUND

In this section we summarize the main theoretical details necessary to compute the decay width within the coupled channels formalism. The main ingredients were already introduced in Ref. [34] to investigate the double fine structure in cold fission. We supposed that both fragments were left in rotational states. In our case the theoretical description becomes simpler, because only the heavy fragment can be excited.

A. Coupled channels formalism

Let us consider an α-decay process

$$P \rightarrow D(J) + \alpha, \tag{1}$$

where J denotes the spin of the rotational state of an even-even nucleus, i.e., $J = 0, 2, 4, 6, \ldots$ We describe the α-core dynamics as in Ref. [34], by using the stationary Schrödinger equation

$$H\Psi(\mathbf{R}, \Omega_D) = E\Psi(\mathbf{R}, \Omega_D), \tag{2}$$

where $\mathbf{R} = (R, \Omega)$ denotes the distance between the centers of two fragments and $E = Q_\alpha$. The orientation of the daughter major axis in the laboratory system is given by Euler angles $\Omega_D = (\varphi_D, \theta_D, 0)$. Because of the fact that all measured decay widths are by many orders of magnitude smaller than the corresponding Q values the stationarity is a very good assumption and an α-decaying state is identified with a narrow resonant solution, containing only outgoing components.

The Hamiltonian describing the α decay in the laboratory system of coordinates is written as follows

$$H = -\frac{\hbar^2}{2\mu}\nabla_R^2 + H_D(\Omega_D) + V(\mathbf{R}, \Omega_D), \tag{3}$$

where μ is the reduced mass of the dinuclear system and H_D describes the rotation of the core. We estimate the interaction between nuclei in terms of the double folding between the nuclear densities [37,38], i.e.,

$$V(\mathbf{R}, \Omega_D) = \int d\mathbf{r}_D \int d\mathbf{r}_\alpha \rho_D(\mathbf{r}_D)\rho_\alpha(\mathbf{r}_\alpha) v(\mathbf{R} + \mathbf{r}_D - \mathbf{r}_\alpha), \tag{4}$$

where v denotes the nucleon-nucleon force. This procedure was widely used to compute the potential between heavy ions by using for their densities a Woods-Saxon shape. In our case the density of the daughter nucleus is given by such a distribution, whereas that of the α particle by a Gaussian with standard parameters [29].

The resulting potential can be divided into a spherical (V_0) and a deformed component (V_d) as follows:

$$V(\mathbf{R}, \Omega_D) = V_0(R) + V_d(\mathbf{R}, \Omega_D). \tag{5}$$

By expanding the nuclear densities in multipoles one obtains the deformed part of the interaction

$$V_d(\mathbf{R}, \Omega_D) = \sum_{\lambda>0} V_\lambda(R)\mathcal{Y}_\lambda(\Omega, \Omega_D). \tag{6}$$

Here the angular part of the wave function has the following ansatz:

$$\mathcal{Y}_\lambda(\Omega, \Omega_D) = [Y_\lambda(\Omega) \otimes Y_\lambda(\Omega_D)]_0. \tag{7}$$

Therefore the rotation of the core is compensated by the rotation of the α particle in the opposite direction. The relation in Eq. (6), with the angular part [Eq. (7)], is nothing else than a multipole-multipole expansion, where the multipole formfactors $V_\lambda(R)$ are given in terms of density distributions [38]. Some authors postulate the radial formfactors in a phenomenological way. In our computations we use the M3Y nucleon-nucleon [39] plus Coulomb force. For details see Ref. [38].

To this potential we also add a simple repulsive core, depending on one independent parameter. The role of this potential is similar to that in Refs. [32–34], where we investigated cold fission. Namely it simulates the Pauli principle and adjusts the energy of the system to the experimental Q value. We show that the total half-life and the partial decay widths do not depend on the shape of this repulsive potential.

If the rotational states of the core belong to the ground band (with the intrinsic angular momentum projection $K = 0$) the wave function is given by a similar superposition, i.e.,

$$\Psi(\mathbf{R}, \Omega_D) = \frac{1}{R}\sum_J f_J(R)\mathcal{Y}_J(\Omega, \Omega_D). \tag{8}$$

The wave functions describing the ground band rotations satisfy the following eigenvalue equations

$$H_D Y_{JM}(\Omega_D) = E_J Y_{JM}(\Omega_D), \tag{9}$$

i.e., they are the normalized Wigner functions with $K = 0$.

By using the orthonormality of angular functions entering the superposition in Eq. (8) one obtains in a standard way the coupled system of differential equations for radial components

$$\frac{d^2 f_J(R)}{d\rho_J^2} = \sum_{J'} A_{JJ'}(R) f_{J'}(R), \tag{10}$$

where the coupling matrix is given by the following:

$$A_{JJ'}(R) = \left[\frac{J(J+1)}{\rho_J^2} + \frac{V_0(R)}{E-E_J} - 1\right]\delta_{JJ'} + \frac{1}{E-E_J}\langle \mathcal{Y}_J | V_d(R) | \mathcal{Y}_{J'}\rangle. \tag{11}$$

Here we introduce the following short-hand notations:

$$\rho_J = \kappa_J R, \quad \kappa_J = \sqrt{\frac{2\mu(E-E_J)}{\hbar^2}}. \tag{12}$$

The matrix element $\langle \mathcal{Y}_J | V_d(R) | \mathcal{Y}_{J'}\rangle$ entering Eq. (11) is given by standard manipulations of angular-momentum algebra. The result is given in terms of the Clebsch-Gordan coefficient as follows:

$$\langle \mathcal{Y}_J | V_d(R) | \mathcal{Y}_{J'}\rangle = \sum_{\lambda>0} V_\lambda(R)\sqrt{\frac{2J+1}{4\pi(2J'+1)}} \times [\langle J, 0; \lambda, 0 | J', 0\rangle]^2. \tag{13}$$

Let us mention that at large distances, where the field becomes spherical and Coulombian the system of equations has a simple form

$$\left[-\frac{d^2}{d\rho_J^2} + \frac{J(J+1)}{\rho_J^2} + \frac{\chi_J}{\rho_J} - 1\right] f_J(\chi_J, \rho_J) = 0, \tag{14}$$

in terms of the so-called Coulomb parameter in the channel J, defined as twice the Sommerfeld parameter

$$\chi_J \equiv 2\frac{Z_\alpha Z_D e^2}{\hbar v_J}. \tag{15}$$

The system of Eq. (10) acquires this form practically beyond $R = R_c + 4\,\mathrm{fm}$, where $R_c = 1.2(A_D^{1/3} + A_\alpha^{1/3})$, because the higher multipoles of the potential $\lambda \neq 0$ are centered around the nuclear surface $R_0 = 1.2A_D^{1/3} \pm 4\,\mathrm{fm}$, as can be seen in Fig. 1.

B. Resonant states

We briefly review the procedure to integrate numerically this system of equations and to find resonant states. We first define N independent column-vector functions, satisfying inside the repulsive core at $R = R_0$, where $V_0(R_0) \gg Q_\alpha$, the following boundary conditions

$$\mathcal{R}_{JI}(R_0) = \delta_{JI}\varepsilon_J, \tag{16}$$

where ε_J are arbitrary small numbers. The index J labels the component, whereas I the solution. If the repulsion is soft then one considers $R_0 = \Delta R$, $\varepsilon_J = (\Delta R)^{J+1}$, where ΔR is the initial integration step.

We also determine N independent outgoing Coulomb column-vector functions satisfying at large distances the system (14), i.e.,

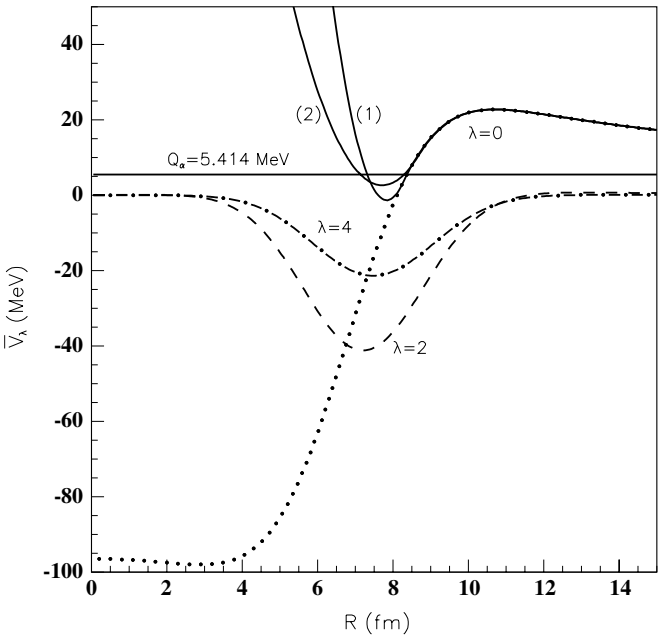

FIG. 1. The radial components of the renormalized α-nucleus potential (30) for $\lambda = 0$ (dots), $\lambda = 2$ (dashes), and $\lambda = 4$ (dot-dashes). The solid pocketlike curves (1) and (2) are the monopole parts of the interaction (31), giving the same Q value. Their parameters are (1) $c = 90.117\,(\mathrm{MeV\,fm^{-2}})$, $Q_\alpha + v_0 = 10.272$ (MeV) and (2) $c = 30.296\,(\mathrm{MeV\,fm^{-2}})$, $Q_\alpha + v_0 = -3.816$ (MeV). The horizontal line denotes the Q value. The decay process is $^{232}\mathrm{Pu} \rightarrow {}^{228}\mathrm{U} + \alpha$.

$$\mathcal{H}_{JI}^{(+)}(R) \equiv \mathcal{G}_{JI}(R) + i\mathcal{F}_{JI}(R) \overset{R\to\infty}{\longrightarrow} \delta_{JI} H_J^{(+)}(\chi_J, \rho_J) \equiv \delta_{JI}\left[G_J(\chi_J, \rho_J) + iF_J(\chi_J, \rho_J)\right], \tag{17}$$

where $G_J(\chi_J, \rho_J)$, $F_J(\chi_J, \rho_J)$ are the irregular and regular spherical Coulomb wave functions, respectively, depending on two independent variables in the channel J. These functions are found by a backward numerical integration.

Each component of the solution is built as a superposition of these N-independent fundamental solutions. We impose the matching boundary decay conditions at the radius R_1 inside the barrier, i.e., to have outgoing waves in all channels

$$f_J(R_1) = \sum_I \mathcal{R}_{JI}(R_1) M_I = \sum_I \mathcal{H}_{JI}^{(+)}(R_1) N_I, \tag{18}$$

and a similar condition for derivatives. The coefficients N_I are nothing else than the scattering amplitudes. These conditions give the following secular equation:

$$\det\begin{bmatrix} \mathcal{R}(R_1) & \mathcal{H}^{(+)}(R_1) \\ d\mathcal{R}(R_1)/dR & d\mathcal{H}^{(+)}(R_1)/dR \end{bmatrix} \approx \det\begin{bmatrix} \mathcal{R}(R_1) & \mathcal{G}(R_1) \\ d\mathcal{R}(R_1)/dR & d\mathcal{G}(R_1)/dR \end{bmatrix} = 0. \tag{19}$$

The first condition is exact and it is fulfilled for complex energies, determining the resonant (Gamow) states. In our case they practically coincide with the real scattering resonant states, because the imaginary parts of energies are much smaller than the corresponding real parts. This corresponds

to vanishing regular Coulomb functions F_J inside the barrier. Therefore the above approximation, given by the second equality, is very good. The roots of the system [Eq. (19)] do not depend on the matching radius R_1 because both internal and external solutions satisfy the same Schrödinger equation.

The coefficients M_I, N_I are fully determined from the normalization of the wave function in the internal region

$$\sum_J \int_{R_0}^{R_2} |f_J(R)|^2 dR = 1, \tag{20}$$

where R_2 is the external turning point. Beyond this radius the wave function has practically vanishing values. This is connected with the fact that all known half-lives in α emission are much larger that the characteristic nuclear time $T_{\min} \approx 10^{-6}\, s \gg T_N \approx 10^{-22}\, s$. Thus, any α-decaying state practically behaves like a bound state, having an exponential decrease versus radius inside the barrier.

One can derive a very useful relation for the scattering amplitude in terms of the wave-function components. By inverting Eq. (18) for some radius $R = R_1$ and then dividing and multiplying the result by $H_I^{(+)}(\rho_I)$ one obtains

$$N_I = \frac{1}{H_I^{(+)}(\rho_I)} \sum_J K_{IJ}(R) f_J(R), \tag{21}$$

where $\rho_I = \kappa_I R$. The propagator operator is defined in such a way that it becomes the unity matrix for a spherical Coulomb field, i.e.,

$$K_{IJ}(R) \equiv H_I^{(+)}(\rho_I)[\mathcal{H}^{(+)}(R)]^{-1}_{IJ} = \delta_{IJ} + \Delta K_{IJ}(R), \tag{22}$$

where $\Delta K_{IJ}(R) \to_{R\to\infty} 0$. Of course the scattering amplitude [Eq. (21)] does not depend on R.

The total decay width is a sum over partial channel widths. It can be derived from the continuity equation in a straightforward way and the result is the following:

$$\Gamma = \sum_J \Gamma_J = \sum_J \hbar v_J \lim_{R\to\infty} |f_J(R)|^2 = \sum_J \hbar v_J |N_J|^2, \tag{23}$$

where v_J is the center-of-mass velocity at infinity in the channel J, i.e.,

$$v_J = \frac{\hbar \kappa_J}{\mu}. \tag{24}$$

We stress on the fact that the wave-function components can be directly recovered by using the experimental information, namely the partial decay widths in Eq. (18)

$$f_J(R) = \sum_I \mathcal{H}^{(+)}_{JI}(R) \sqrt{\frac{\Gamma_I}{\hbar v_I}}, \tag{25}$$

because the matrix $\mathcal{H}^{(+)}$, defined by Eq. (17), is fully determined by the potential. Of course the wave function depends on the details of the used interaction. This is the main reason why we prefer to characterize the fine structure by the quantities

$$I_J \equiv \log_{10} \frac{\Gamma_0}{\Gamma_J}, \tag{26}$$

instead of the hindrance factors, defined as $HF(J) = |f_0/f_J|^2$, and that are model dependent.

III. INFLUENCE OF POTENTIAL PARAMETERS ON THE FINE STRUCTURE

First, let us analyze the sentivity of the α-decay fine structure on different parameters entering the potential [Eq. (4)]. We describe the density of the daughter nucleus by an axially deformed Woods-Saxon shape, i.e.,

$$\rho_{D,\tau}(\mathbf{r}_D) = \frac{\rho^{(0)}_{D,\tau}}{1 + e^{[r_D - R_{0,\tau}(\Omega_D)]/a}}, \tag{27}$$

where the radius of the nuclear surface is given by the following:

$$R_{0,\tau}(\Omega_D) = R_{0,\tau}\left[1 + \beta_2 Y_{20}(\Omega_D) + \beta_4 Y_{40}(\Omega_D)\right], \tag{28}$$

and the central densities are normalized by the total number of protons ($\tau = \pi$) and neutrons ($\tau = \nu$) separately. The α-particle density is given by a Gaussian distribution as follows:

$$\rho_\alpha(\mathbf{r}_\alpha) = \frac{4}{b^3 \pi^{3/2}} e^{-(r_\alpha/b)^2}. \tag{29}$$

Concerning the α-nucleus interaction we multiplied the double folding integral [Eq. (6)] by a strength parameter v_a, to achieve the well-known relation between the half-life and Q value. This relation is mainly given by the ratio between the Q value and the height of the repulsive barrier and we show later that one should consider a quenching factor, i.e., $v_a < 1$. The necessity to use such a factor multiplying the double folded α-daughter potential was already stressed in Refs. [27,28]. It is connected with the fact that the parameters of the used M3Y interaction were fitted from scattering experiments involving heavy ions [37,39]. Thus, the renormalized multipoles of the interaction are given by the following:

$$\overline{V}_\lambda(R) = v_a V_\lambda(R). \tag{30}$$

They are plotted in Fig. 1. By dots we indicated the monopole component $\lambda = 0$, by dashes $\lambda = 2$ and by dot-dashes $\lambda = 4$ components, respectively. The horizontal solid line indicates the Q value of the process, which in our case is $^{232}\mathrm{Pu} \to {}^{228}\mathrm{U} + \alpha$. To obtain the experimental value of the half-life we used for the quenching factor $v_a = 0.62$. We also used the standard value of the diffusivity $a = 0.5$ fm, the α-particle size parameter $b = 1.19$ fm [29] and the deformations β_2, β_4 given by the systematics of Ref. [40].

This interaction is able to describe the α-daughter system for large distances $R > R_m$. To describe the internal two-body dynamics we used a repulsive core, taking care on the fact that an α-particle exists only on the nuclear surface. Indeed, microscopic computations, see, e.g., Fig. 2(a) of Ref. [6], suggest that the α-particle wave function is peaked in the region of the nuclear surface and it has a Gaussian-like shape. Moreover, the monopole component represents more than 90% of the total amount. Such a wave function corresponds to a shifted harmonic oscillator potential, which we have to consider in the internal region $R \leqslant R_m$, i.e.,

$$\begin{aligned} \overline{V}_0(R) &= v_a V_0(R),\ R > R_m \\ &= c(R - R_0)^2 - v_0,\ R \leqslant R_m. \end{aligned} \tag{31}$$

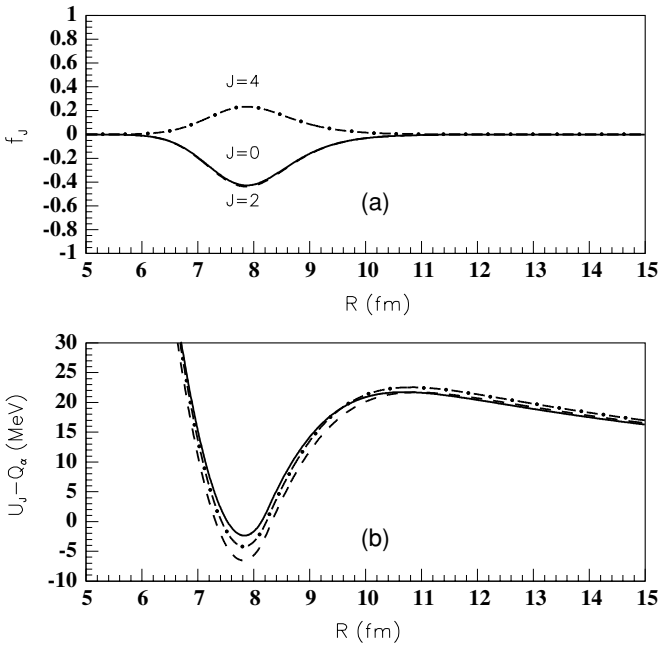

FIG. 2. (a) The radial components of the α-nucleus wave function inside the pocketlike potential for $J = 0$ (solid line), $J = 2$ (dashes), and $J = 4$ (dot-dashes). (b) The radial dependence of the diagonal α-nucleus matrix elements plus the centrifugal barrier [Eq. (33)] for $J = 0$ (solid line), $J = 2$ (dashes), and $J = 4$ (dot-dashes). In Fig. 1 the repulsive core is labeled (1). The decay process is $^{232}\mathrm{Pu} \rightarrow {}^{228}\mathrm{U} + \alpha$.

This interaction is given in Fig. 1 by two pocketlike curves. The curves labeled (1) and (2) give the same Q value. Their parameters are as follows: (a) $c = 90.117\,(\mathrm{MeV\,fm^{-2}})$, $Q_\alpha + v_0 = 10.272$ (MeV) and (b) $c = 30.296\,(\mathrm{MeV\,fm^{-2}})$, $Q_\alpha + v_0 = -3.816$ (MeV).

We considered the quantity $Q_\alpha + v_0$ because it is the excitation energy inside the pocketlike interaction. From this figure it is clear that if one considers a deformed part for repulsive multipoles with $\lambda \neq 0$ the effect can be renormalized by the monopole repulsion in the internal region $R < R_0 = 1.2A_D^{1/3}$.

We stress the fact that only three parameters, namely v_a, v_0, and c, are independent, because the radii R_0 and R_m are determined by using the matching conditions

$$\begin{aligned} v_a V_0(R_m) &= c(R_m - R_0)^2 - v_0 \\ v_a \frac{dV_0(R_m)}{dR} &= 2c(R_m - R_0). \end{aligned} \tag{32}$$

These conditions allows us to write down a single equation determining the matching radius for some given combination of v_a, v_0, c. The parameters of the repulsive cores (1) and (2) in Fig. 1 were chosen to give the best fit simultaneously for Q_α, Γ_J, $J = 0, 2, 4$.

This procedure to estimate the repulsive core is different from that of our previous references [22,33,34], where we used the same double folding procedure for a δ-like interaction. The advantage of the method used in this article is that we completely decouple the internal repulsion from the external

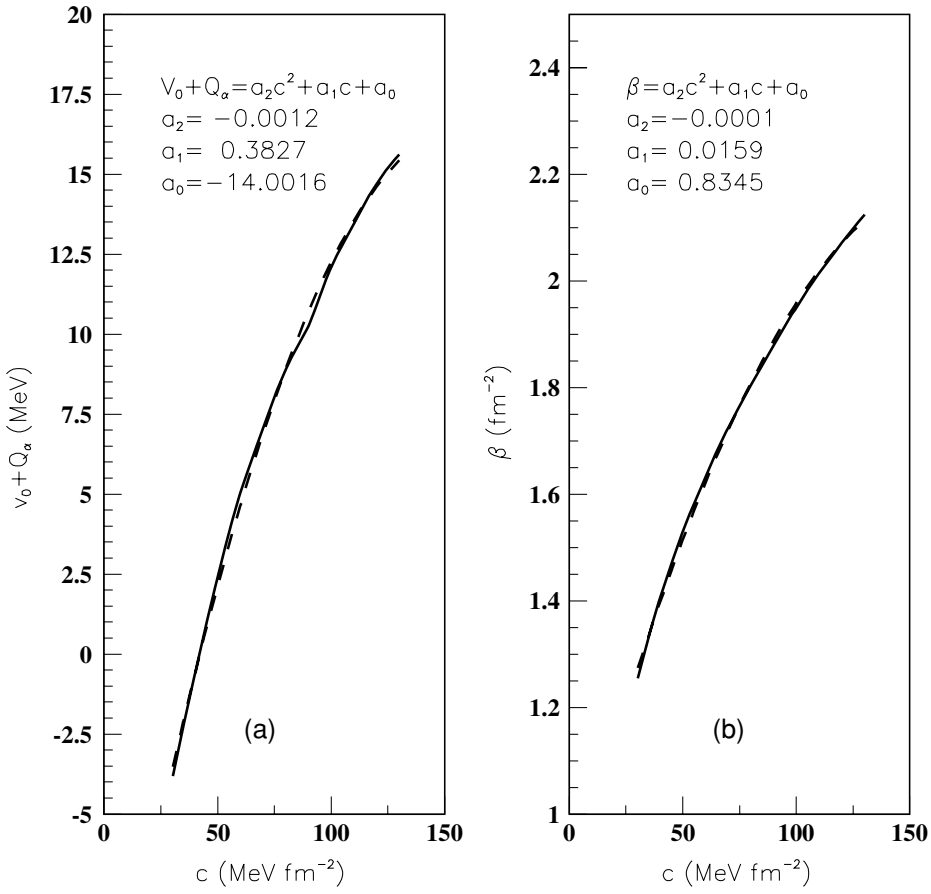

FIG. 3. (a) The dependence of the quantity $v_0 + Q_\alpha$ on the parameter c of the repulsive core defined by Eq. (31) (solid line). By dashes is given the quadratic fit. The fit parameters are given. (b) The dependence of the h.o. parameter for the monopole α-particle wave function defined by Eq. (34) versus the same parameter c (solid line). The parameters of the quadratic fit (dashes) are given. The decay process is $^{232}\mathrm{Pu} \rightarrow {}^{228}\mathrm{U} + \alpha$.

part and thus we are able to control the repulsive and atractive parameters independently, at variance with the δ-like force.

In Fig. 2(a) we plotted the radial components of the wave function for $J = 0$ (solid line), $J = 2$ (dashes), and $J = 4$ (dot-dashes), corresponding to the pocketlike repulsion (1) in Fig. 1. In Fig. 2(b) we give the radial dependencies of the diagonal terms [with the same symbols as in (a)], corresponding to the α-daughter potential plus the centrifugal barrier, i.e.,

$$U_J(R) = \langle \mathcal{Y}_J | \overline{V}(R) | \mathcal{Y}_J \rangle + \frac{\hbar^2 J(J+1)}{2\mu R^2} = \frac{1}{\sqrt{4\pi}} \sum_\lambda \overline{V}_\lambda(R) \left[\langle J, 0; \lambda, 0 | J, 0 \rangle \right]^2 + \frac{\hbar^2 J(J+1)}{2\mu R^2}. \quad (33)$$

Thus, in the spherical case, where the components with $\lambda > 0$ vanish, the decay widths to excited states are entirely determined by the corresponding centrifugal barriers.

An interesting observation is conected with the shape of the pocketlike potentials (1) and (2) in Fig. 1. The repulsive strength c and the quantity $Q_\alpha + v_0$ are strongly related and therefore the repulsive core is charactized by one independent parameter. Indeed, by increasing c one should simultaneously increase the excitation energy $Q_\alpha + v_0$, to obtain the same Q value and therefore the total half-life. This dependence is shown in Fig. 3(a). The parameters of the already mentioned curves (1) and (2) belong to this line.

In Fig. 3(b), we also plotted the width β of the monopole radial wave function component, shown in Fig. 2(a), as a function of the repulsive strength c. The width is obtained by fitting this component with a Gaussian, i.e.,

$$\frac{f_0(R)}{R} \approx A_0 e^{-\beta(R-R_0)^2/2}. \quad (34)$$

Moreover, our computations showed that the total half-life and the fine structure, defined by (26), is weakly affected by simultaneously changing the parameters of the repulsive potential for this decay process. This is shown in Fig. 4.

The importance of the quenching strength v_a is shown in Fig. 5. We plotted here with a solid line the Q value, with dots $\log_{10} T$, with a dashed line I_2, and with a dot-dashed line I_4, as a function of v_a, by considering fixed the parameters of the repulsive potential, i.e., $Q_\alpha + v_0 = 10.272$, $c = 90.117$. One sees a strong dependence of the first two quantities and a weaker variation for I_4, whereas I_2 is practically a constant. We stress that at the value $v_a \approx 0.62$ one obtains simultaneously the best fit with the experimental data (shown by short horizontal lines) for all considered quantities.

Once this parameter is fixed, we can adjust the Q values for different decays by using one parameter, namely the repulsive depth v_0, because for a given quenching strength v_a the repulsive strength c has a definite value. As mentioned above, we consider as an independent parameter the sum

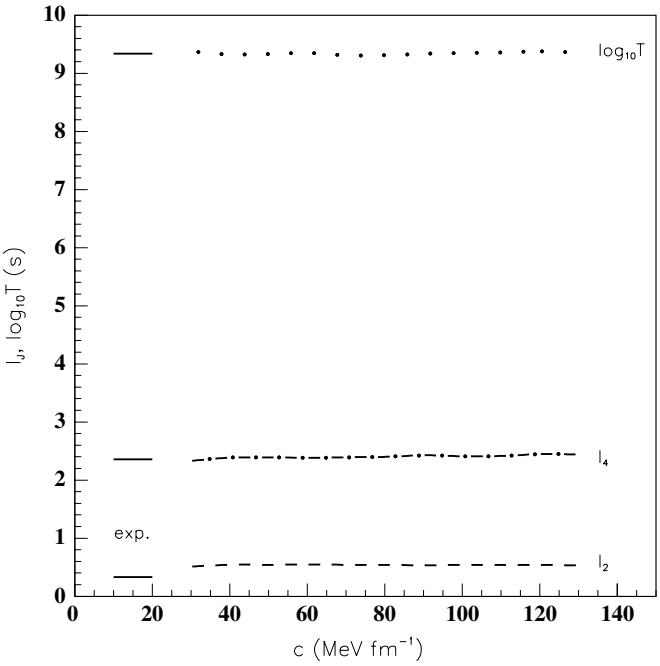

FIG. 4. The dependence of the ratios I_J, defined by Eq. (26) for $J = 2$ (dashed line) and $J = 4$ (dot-dashed line) upon the repulsive strength parameter c, when the parameter $v_0 + Q_\alpha$ simultaneously changes according to the curve in Fig. 3(a). The dependence between the logarithm of the total half-life versus c is plotted with dots. On the left side we give the corresponding experimental values. The decay process is $^{232}\mathrm{Pu} \rightarrow {}^{228}\mathrm{U} + \alpha$.

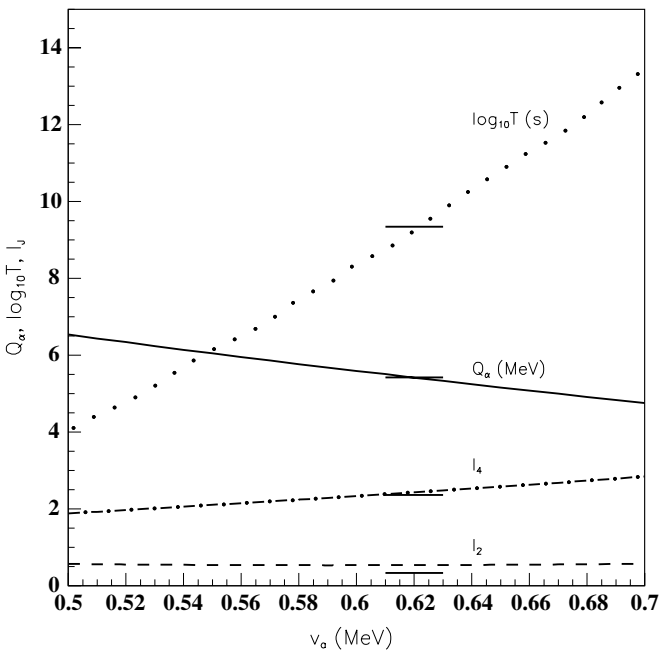

FIG. 5. The Q value (solid line), the logarithm of the total half-life (dots), I_2 (dashes) and I_4 (dot-dashes) versus the attraction strength v_a. The other potential parameters are $c = 90.117$ (MeV fm^{-2}), $Q_\alpha + v_0 = 10.272$ (MeV). The corresponding experimental values are shown by short horizontal lines. The decay process is $^{232}\mathrm{Pu} \rightarrow {}^{228}\mathrm{U} + \alpha$.

TABLE I. Experimental data for α decays from rotational nuclei: deformations, excitation energies, logarithm of the relative intensities, logarithm of the total half-life and Q value. The calculated data correspond to a variable quenching parameter v_a (labeled with a superscript a), or to a variable size parameter of the α-cluster density (labeled with a superscript b).

n	Z	A	β_2	β_4	E_2 (keV)	E_4 (keV)	I_2	I_2^a	I_2^b	I_4	I_4^a	I_4^b	$\log_{10} T$ (s)	$\log_{10} T_a$ (s)	$\log_{10} T_b$ (s)	Q_α (MeV)
1	90	226	0.173	0.111	72.200	226.430	0.324 *4*	0.602	0.594	2.25 *5*	2.415	2.426	6.26 *5*	6.323	6.281	5.993
2	90	228	0.182	0.112	57.759	186.823	0.335 *4*	0.556	0.538	2.36 *3*	2.364	2.419	9.336 *3*	9.321	9.423	5.414
3	90	230	0.198	0.115	53.200	174.100	0.400 *2*	0.565	0.536	2.55 *3*	2.519	2.610	12.889 *2*	12.871	12.815	4.859
4	90	232	0.207	0.108	49.369	162.120	0.46 *8*	0.572	0.534	2.45 *3*	2.530	2.663	14.869 *1*	14.870	14.935	4.572
5	90	234	0.215	0.102	49.550	163.000	0.58 *6*	0.622	0.572	3.01 *7*	2.673	2.835	17.149 *1*	17.299	17.354	4.270
6	92	230	0.199	0.115	51.720	169.500	0.3 *3*	0.429	0.399	2.2 *3*	2.072	2.157	5.723 *5*	5.645	5.566	6.310
7	92	232	0.207	0.117	47.572	156.570	0.355 *7*	0.429	0.388	2.6 *3*	2.125	2.247	7.955 *2*	7.912	7.782	5.867
8	92	234	0.215	0.110	43.498	143.351	0.389 *2*	0.427	0.378	2.83 *3*	2.099	2.259	9.442 *1*	9.274	9.298	5.593
9	92	236	0.215	0.102	45.242	149.476	0.429 *2*	0.480	0.418	2.932 *7*	2.182	2.373	11.329 *1*	11.357	11.304	5.256
10	92	238	0.215	0.093	44.910	148.410	0.513 *4*	0.519	0.446	3.40 *2*	2.215	2.435	13.073 *3*	13.020	13.101	4.984
11	94	236	0.215	0.110	44.630	147.450	0.391*13*	0.387	0.328	3.1 *3*	1.939	2.137	6.37 *2*	5.981	6.030	6.397
12	94	238	0.215	0.102	44.080	145.960	0.456 *2*	0.409	0.339	3.33 *3*	1.926	2.155	7.148 *1*	6.972	6.985	6.216
13	94	240	0.223	0.087	42.824	141.690	0.51 *3*	0.438	0.356	3.54 *3*	1.922	2.170	8.757 *3*	8.533	8.540	5.902
14	94	242	0.224	0.071	44.540	147.300	0.67 *3*	0.509	0.412	3.3 *5*	1.988	2.251	11.177 *4*	10.969	11.011	5.475
15	94	244	0.224	0.071	46.000	156.900	0.657 *6*	0.552	0.444	3.03 *7*	2.098	2.391	13.041 *8*	12.930	12.964	5.162
16	96	242	0.224	0.079	42.130	138.000	0.59 *3*	0.399	0.305	2.72 *6*	1.706	1.974	5.109 *7*	4.941	4.796	6.862
17	96	244	0.234	0.073	42.965	142.348	0.61 *3*	0.431	0.330	2.3 *3*	1.785	2.088	7.460 *4*	7.164	7.163	6.361
18	96	246	0.234	0.057	42.852	142.010	0.752 *7*	0.476	0.359	2.5 *3*	1.760	2.070	8.616 *3*	8.295	8.363	6.128
19	96	248	0.234	0.040	42.380	143.800	0.729 *9*	0.514	0.375	2.55 *8*	1.680	1.983	7.935 *2*	7.923	7.770	6.217
20	98	248	0.235	0.040	41.530	137.810	0.748 *7*	0.457	0.320	1.94 *2*	1.504	1.807	4.961 *1*	4.585	4.343	7.153
21	98	250	0.245	0.026	42.722	141.885	0.777*10*	0.475	0.327	2.02 *4*	1.454	1.768	4.067 *1*	3.842	3.698	7.307

$Q_\alpha + v_0$, because it gives the energy of the first excitation in the pocketlike potential.

IV. SYSTEMATICS OF THE FINE STRUCTURE

We analyzed α decays for 20 rotational nuclei with known ratios I_2 and I_4, and one where I_4 was only given as a limit. The experimental data, namely the excitation energies, total half-lives and Q values, are taken from the compilation [36]. We also compared fine structure intensities for $J = 2^+$, $J = 4^+$ states and total half-lives, with respective uncertainties, with the ENSDF database. Only one of the half-lives, namely ^{240}Pu, slightly differs from the value of Ref. [36]. The deformation parameters were taken from the systematics in Ref. [40]. These data for daughter nuclei are given in Table I.

Concerning the experimental errors, given by italic characters in Table I, we make the following observations. The errors for the 4^+ intensity were not given for the decays to ^{230}U, ^{232}U, ^{236}Pu, and ^{246}Cm. In these cases we considered relative uncertainty of 4^+ intensity to be 50%, as in ^{244}Cm measurement. For ^{242}Pu 4^+ the intensity was not given. We estimated the intensity limit and the uncertainty is taken to be 100%. The uncertainty of ^{230}U half-life was taken arbitrarily 10%, as in Ref. [36]. The uncertainty for α-decay intensity to 2^+ state in ^{230}U was not given, so that we considered the relative uncertainty to be 50%.

In Fig. 6(a) we plotted by squares the experimental Q values versus the number of the decay process, given in the first column of Table I. In the lower part [Fig. 6(b)] we give the logarithm of experimental half-lives by squares. In Fig. 7(a) shows the quadrupole (squares) and hexadecapole deformations (triangles), whereas in Fig. 7(b) the experimental values of the ratios I_2 and I_4 (squares).

The results of our computations are given in Figs. 6 and 7 by open circles and in Table I. It turns out that, to satisfy the relation between the half-life and Q value, the quenching strength should slowly decrease from $v_a \approx 0.6$ for $A = 226$ to $v_a \approx 0.5$ for $A = 250$. Thus, we introduced a linear decrease using the relation $v_a = 0.668 - 0.004\,(A - 208)$. In table the results are labeled with a. The value of the repulsive strength was taken $c = 100$ MeV fm^{-2}. As mentioned, we adjusted the energy of the first resonant state in the pocketlike potential by using the repulsive depth v_0, which is plotted in Fig. 6(a) with open circles.

The variation of this parameter can be correlated with the Q values in the same figure and it has an important consequence. It is known that the width of the Gaussian, fitting the microscopic preformation amplitude of the α particle, has practically no variation along any isotope chain [6]. However, according to Figs. 6(a) and 3(b) the width of the wave function within the present approach has a strong variation with the Q value. This feature is an evidence for the α-clustering phenomenon on the nuclear surface, in

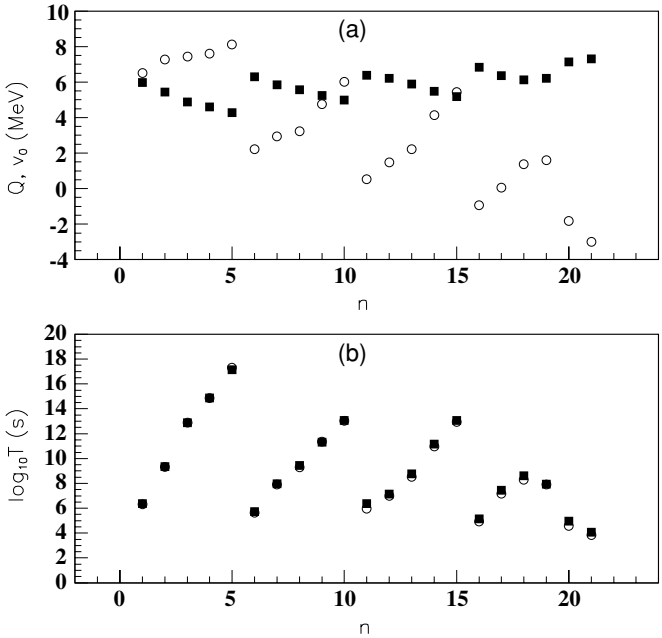

FIG. 6. (a) Q value (squares) and the depth of the repulsive potential v_0 (open circles) versus the decay number given by the first column in Table I. The attractive quenching parameter is given by the rule $v_a = 0.668 - 0.004\,(A - 208)$. (b) Logarithm of experimental half-lives (squares) and the corresponding computed values (open circles). In table the corresponding data are labeled with a superscript a.

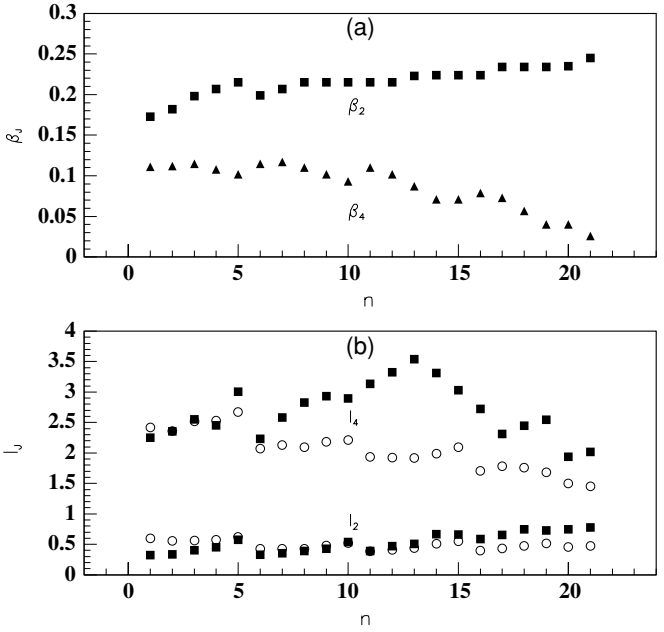

FIG. 7. (a) Deformation parameters β_2 (squares) and β_4 (triangles) versus the decay number given by the first column in Table I. (b) Experimental ratios I_2, I_4 defined by Eq. (26) (squares) and the corresponding computed values (open circles). The attractive quenching parameter is given by the rule $v_a = 0.668 - 0.004\,(A - 208)$. In Table I the corresponding data are labeled with a superscript a.

addition to the α preformation predicted by the standard shell model.

From Fig. 6(b) one sees that the computed half-lives (open circles) practically reproduce the experimental values. In Fig. 7(b) we show via open circles the results for I_2 and I_4. One sees that we obtained good agreement with experimental data for I_2. Concerning I_4, very good agreement was achieved only for the $Z = 90$ isotope chain. For the last $Z = 96$ and $Z = 98$ chains the agreement is within a half-order of magnitude, whereas the central peak, around the $Z = 94$ chain, is not reproduced. The difference between experiment and theory in this region is about 1.5 orders of magnitude.

The following observation is interesting. The main trend of the experimental and computed I_2 values in Fig. 7(b) is clearly correlated with the quadrupole deformation in Fig. 7(a). The same is true, but mainly for the computed I_4 values, which are correlated with β_4 in Fig. 7(a). This correlation between I_J and β_J can be understood from Eq. (33), expressing the barriers and therefore the penetrabilities for each partial wave, as a sum of all multipole terms. Thus, the existence of the central peak for experimental I_4 data corresponding to the neutron chain $Z = 94$ seems to be out of the correlation between the fine structure and deformation parameters. At this moment we have no explanation for this experimental feature.

The correlation between decay widths and deformation parameters seems to be an universal property of emission processes. This feature was already evidenced for α decays between ground states in Ref. [6]. However, the protons are emitted with given angular momenta from some proton-rich nuclei. Recently we found an almost 100% correlation between the quadrupole deformation and half-lives, corrected by the centrifugal barrier, in all measured proton emitters [41].

We have also checked higher resonances in the pocketlike potential, but, because the orthogonality with respect to the first state, they give a totally different picture of the fine structure, compared with experimental data.

The variation of the quenching parameter v_a by increasing the mass number corresponds to the change of the Coulomb barrier because of the nuclear part. Indeed the pure Coulomb barrier, according to Eq. (14) and $\chi \sim Z/\sqrt{Q_\alpha}$, would give the following dependence of the total half-life

$$\log_{10} T = c_1 \frac{Z}{\sqrt{Q_\alpha}} + c_2. \tag{35}$$

In reality the Viola-Seaborg empirical rule postulates a more complex dependence [42]

$$\log_{10} T = \frac{a_1 Z + a_2}{\sqrt{Q_\alpha}} + a_3 Z + a_4. \tag{36}$$

Thus, the influence of the internal nuclear part is expressed by the additional term $a_2/\sqrt{Q_\alpha} + a_3 Z$. In connection with this observation we have checked that a similar rule for the quenching factor depending on the charge number, i.e., $v_a = 0.7 - 0.125\,(Z - 82)$, gives very close results, which practically cannot be distinguished from theoretical results in Fig. 6(b), in comparison with the dependence on the mass number. Anyway, we should stress the fact that our description

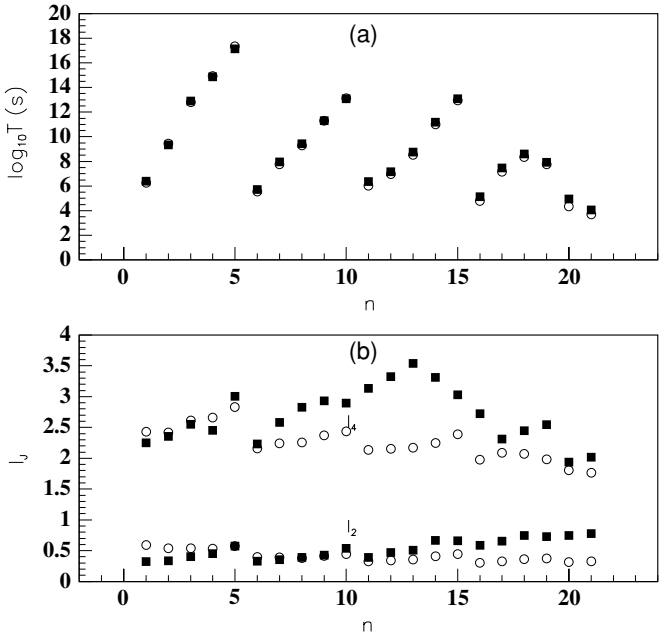

FIG. 8. (a) Logarithm of experimental half-lives (squares) and the corresponding computed values (open circles). The α-particle size parameter [Eq. (29)] is given by the rule $b = 1.744 - 0.032(A - 208)$ and the quenching parameter is $v_a = 0.6$. (b) Experimental ratios I_2, I_4 (squares) and the corresponding computed values (open circles). In Table I the corresponding data are labeled with a superscript b.

depends on only two parameters instead of four parameters in Eq. (36).

This effect can be also explained by considering an alternative picture, namely by changing the diffusivity parameter b of the α particle in Eq. (29) according to the rule $b = 1.744 - 0.032\,(A - 208)$, for a constant value $v_a = 0.6$. Microscopic estimates show that the change of the daughter nuclear difusivity should be very small. In this way the width of the α cluster in the surface region should decrease by increasing the mass number of the daughter nucleus to reproduce the total half-lives, as can be seen in Fig. 8(a) (open circles). The results are labeled in Table I by the index (b). In Fig. 8(b) the fine structure I_J is shown with open circles by considering the above change of the cluster size parameter. One sees that the values for I_4 are slightly improved with respect to those in Fig. 7(b).

As mentioned, one has a dependence of the cluster width on the Q value. Therefore there is a possible additional change of the cluster size in the region of the nuclear surface because of the dependence of the Coulomb barrier on the mass (or charge) number. A definite answer to the question: the effective nucleon-nucleon interaction or the size of the α-particle changes in the nuclear surface region, still remains open, because both approaches give qualitatively the same results. Anyway, this problem concerns fundamental aspects of the effective nuclear interaction and its dependence on the α clustering and thus gives the possibility to express the empirical parameters of the Viola-Seaborg rule in terms of microscopic parameters.

Our simple model is able to explain quantitatively the fine structure to $J = 2^+$ states, namely that the decay widths to $J = 2^+$ states are by 0.5 orders of magnitude smaller than the ones for transitions between ground states. At the same time it is able to explain the fact that most of the decay widths to $J = 4^+$ states are by 2.5 orders of magnitude smaller with respect to the widths between ground states.

V. CONCLUSIONS

We used in this article a simple model to explain the α-decay fine structure in rotational nuclei. We considered the coupled channels formalism to estimate decay widths and the double folding procedure to compute the interaction between the daughter plus α-particle. The daughter nucleus has as eigenstates the standard $K = 0$ Wigner functions. We considered as an effective particle-particle nuclear interaction the superposition of three Yukawa terms (M3Y), able to describe scattering data. The Q value of the system is reproduced by adjusting the depth of a parabolic repulsive core, simulating the Pauli principle. The decaying state was indentified with the first resonance in the resulting pocketlike potential.

It turned out that this simple rotational model is able to explain very well total half-lives and decay widths to the first 2^+ states, as soon as the basic M3Y interaction is quenched by a factor v_a whose value decreases with increasing mass number. Consequently the Coulomb barrier should increase. This effect can be also reproduced by keeping a constant value $v_a = 0.6$ and by changing the size of the α-cluster density as a function of the mass number. It is interesting to mention that the obtained results do not depend on the parameters of the repulsive potential. Does the effective nucleon-nucleon interaction or the size of the α-particle in the nuclear surface region change? This still remains an open question, because both approaches give qualitatively the same results. In any case, this analysis clearly shows that the effective nucleon-nucleon interaction is influenced by α clustering and this dependence changes with the mass number.

Concerning the decay widths to 4^+ rotational states we obtained a good agreement with experimental data for the lightest $Z = 90$ neutron chain and a satisfactory agreement for $Z = 92, 96$, and 98 chains. This simple model is able to qualitatively explain the gross feature of the fine structure, but still the computed values in the region around $Z = 94$ chain differ from experimental data by 1.5 orders of magnitude. It is an interesting observation that our theoretical results concerning I_J are proportional to the corresponding deformations β_J, whereas the experimental values of I_4 for the $Z = 94$ chain do not satisfy this rule. At this moment we have no explanation for this effect, which is not connected with the deformed neutron magic number $N = 152$.

We also stress on the fact that the parameters of the nucleon-nucleon interaction were fitted by using heavy ions scattering data. These experiments can probe potentials only in the region of the Coulomb barrier. However, the α decay is

a deep subbarrier process at low energies, where the scattering has a purely Rutherford pattern. Thus, α-decay fine structure is potentially a valuable tool to probe the nuclear interaction in the internal region. It is in principle able to improve our knowledge about how the effective nucleon-nucleon potential changes in the presence of α clustering.

[1] G. Gamow, Z. Phys. **51**, 204 (1928).
[2] R. G. Thomas, Prog. Theor. Phys. **12**, 253 (1954).
[3] A. M. Lane and R. G. Thomas, Rev. Mod. Phys. **30**, 257 (1958).
[4] H. J. Mang, Annu. Rev. Nucl. Sci. **14**, 1 (1964).
[5] J. K. Poggenburg, H. J. Mang, and J. O. Rasmussen, Phys. Rev. **181**, 1697 (1969).
[6] D. S. Delion, A. Săndulescu, and W. Greiner, Phys. Rev. C **69**, 044318 (2004).
[7] J. O. Rasmussen, Phys. Rev. **113**, 1593 (1959).
[8] A. Săndulescu and O. Dumitrescu, Phys. Lett. **19**, 404 (1965).
[9] A. Săndulescu and O. Dumitrescu, Phys. Lett. **B24**, 212 (1967).
[10] M. I. Cristu, O. Dumitrescu, N. I. Pyatov, and A. Săndulescu, Nucl. Phys. **A130**, 31 (1969).
[11] D. S. Delion, A. Florescu, M. Huyse, J. Wauters, P. Van Duppen, ISOLDE Collaboration, A. Insolia, and R. J. Liotta, Phys. Rev. Lett. **74**, 3939 (1995); Phys. Rev. C **54**, 1169 (1996).
[12] J. Wauters *et al*., Z. Phys. A **342**, 277 (1992).
[13] J. Wauters *et al*., Z. Phys. A **344**, 29 (1992).
[14] J. Wauters *et al*., Z. Phys. A **345**, 21 (1993).
[15] J. Wauters, P. Dendooven, M. Huyse, G. Reusen, P. Van Duppen, P. Lievens, and ISOLDE Collaboration, Phys. Rev. C **47**, 1447 (1993).
[16] J. Wauters, N. Bijnens, H. Folger, M. Huyse, H. Y. Hwang, R. Kirchner, J. von Schwarzenberg, and P. Van Duppen, Phys. Rev. C **50**, 2768 (1994).
[17] J. Wauters *et al*., Phys. Rev. Lett. **72**, 1329 (1994).
[18] N. Bijnens *et al*., Phys. Rev. Lett. **75**, 4571 (1995).
[19] R. G. Allatt *et al*., Phys. Lett. **B437**, 29 (1998).
[20] C. F. Liang, R. K. Sheline, P. Paris, M. Hussonnois, J. F. Ledu, and D. B. Isabelle, Phys. Rev. C **49**, 2230 (1994).
[21] D. S. Delion and R. J. Liotta, Phys. Rev. C **56**, 1782 (1997).
[22] D. S. Delion and J. Suhonen, Phys. Rev. C **64**, 064302 (2001).
[23] S. Peltonen, D. S. Delion, and J. Suhonen, Phys. Rev. C **71**, 044315 (2005).
[24] J. O. Rasmussen and B. Segal, Phys. Rev. **103**, 1298 (1956).
[25] H. M. A. Radi, A. A. Shihab-Eldin, J. O. Rasmussen, and Luiz F. Oliveira, Phys. Rev. Lett. **41**, 1444 (1978).
[26] P. O. Fröman, Mat. Fys. Skr. Dan. Vid. Selsk. **1**, 3 (1957).
[27] R. Neu and F. Hoyler, Phys. Rev. C **46**, 208 (1992).
[28] H. Abele and G. Staudt, Phys. Rev. C **47**, 742 (1993).
[29] Dao T. Khoa, Phys. Rev. C **63**, 034007 (2001).
[30] D. N. Basu, J. Phys. G **29**, 2079 (2003).
[31] Y. K. Gambhir, A. Bhagwat, M. Gupta, and Arun K. Jain, Phys. Rev. C **68**, 044316 (2003).
[32] D. S. Delion, A. Săndulescu, S. Mişicu, F. Cârstoiu, and W. Greiner, Phys. Rev. C **64**, 041303(R) (2001).
[33] D. S. Delion, A. Săndulescu, S. Mişicu, F. Cârstoiu, and W. Greiner, J. Phys. (London) G **28**, 289 (2002).
[34] D. S. Delion, A. Săndulescu, and W. Greiner, Phys. Rev. C **68**, 041303(R) (2003).
[35] A. Săndulescu, A. Florescu, F. Cârstoiu, W. Greiner, J. H. Hamilton, A. V. Ramayya, and B. R. S. Babu, Phys. Rev. C **54**, 258 (1996).
[36] Y. A. Akovali, Nucl. Data Sheets **84**, 1 (1998).
[37] G. R. Satchler and W. G. Love, Phys. Rep. **55**, 183 (1979).
[38] F. Cârstoiu and R. J. Lombard, Ann. Phys. (NY) **217**, 279 (1992).
[39] G. Bertsch, J. Borysowicz, H. McManus, and W. G. Love, Nucl. Phys. **A284**, 399 (1977).
[40] P. Möller, J. R. Nix, W. D. Myers, and W. J. Swiatecki, At. Data Nucl. Data Tables **59**, 185 (1995).
[41] D. S. Delion, R. J. Liotta, and R. Wyss, Phys. Rev. Lett. (in press).
[42] V. E. Viola and G. T. Seaborg, J. Inorg. Nucl. Chem. **28**, 741 (1966).